arXiv:1609.06356v1 [cond-mat.mes-hall] 20 Sep 2016

Review on carrier multiplication in graphene

Ermin Malic[1],* Torben Winzer[2], Florian Wendler[2], and Andreas Knorr[2]
[1] *Department of Physics, Chalmers University of Technology, 41296 Gothenburg, Sweden and*
[2] *Department for Theoretical Physics, Technical University Berlin, 10623 Berlin, Germany*

The remarkable gapless and linear band structure of graphene opens up new carrier relaxation channels bridging the valence and the conduction band. These Auger scattering processes change the number of charge carriers and can give rise to a significant multiplication of optically excited carriers in graphene. This is an ultrafast many-particle phenomenon that is of great interest both for fundamental many-particle physics as well as technological applications. Here, we review the research on carrier multiplication in graphene and Landau-quantized graphene including theoretical modelling and experimental demonstration.

The most fascinating ultrafast phenomenon characterizing the carrier dynamics in graphene is the appearance of carrier multiplication (CM), i.e. generation of multiple electron-hole pairs through internal scattering[1]. The underlying physical mechanism of this phenomenon are Auger processes, which are specific Coulomb interband scattering events, where one carrier (electron or hole) bridges the valence and the conduction band, while the other involved carrier remains in the same band, cf. Fig. 1(a). As a result, Auger scattering changes the overall charge carrier density consisting of electrons in the conduction and holes in the valence band. We distinguish Auger recombination (AR) and the inverse process of impact excitation (IE)[2]. The latter inreases, while the first reduces the number of carriers. The efficiency of the two Auger processes depends on the excitation regime and the resulting Pauli blocking. After a weak optical excitation, the probability of the interband process close to the Dirac point is higher for IE, since here an electron from the almost full valence band scatters into the weakly populated conduction band, cf. Fig. 1(b). The inverse process of AR is strongly suppressed by Pauli blocking. As a result, carrier multiplication can take place[3,4].

The theoretical prediction of carrier multiplication for semiconductor quantum dots in 2002[1] and its experimental verification two years later[5] has attracted much attention[6–11]. Since then, the concept has been extended to other nanomaterials including carbon nanotubes and graphene[3,12–19]. This ultrafast phenomenon has the potential to increase the power conversion efficiency of single-junction solar cells[20] above the Shockley-Queisser limit[21]. Moreover, carrier multiplication enables a fast detection of photons with a high responsivity. In graphene, the occurrence of carrier multiplication has been recently theoretically predicted[3,4,22,23] and experimentally confirmed[17,19,24,25]. Furthermore, Landau-quantized graphene exhibiting an externally tunable bandgap has been suggested to exploit this effect for designing graphene-based photovoltaic devices. In spite of the non-equidistant Landau quantization, Auger scattering has been theoretically and experimentally demonstrated to be the crucial relaxation channel[26] resulting in a carrier multiplication[18].

To microscopically access the ultrafast carrier dynamics in graphene including the phenomenon of carrier multiplication, we have developed a theoretical approach based on graphene Bloch equations within the second-order Born Markov approximation[2,27–30]. This system of coupled equations of motion for carrier occupation $\rho^{\lambda}_{\mathbf{k}}(t)$, microscopic polarization $p_{\mathbf{k}}(t)$, and phonon number $n^{j}_{\mathbf{q}}$ include contributions from carrier-light, carrier-carrier, and carrier-phonon interaction on a consistent microscopic footing. Here, the electronic and phonon momentum are denoted by $\mathbf{k}$ and $\mathbf{q}$, furthermore, $\lambda = c, v$ stands for the conduction (c) or valence (v) band, and j describes the considered optical or acoustic phonon modes. Solving the graphene Bloch equations, we have access to the temporal evolution of the carrier density $\mathcal{N}(t)$ at different excitation conditions allowing us to address the question whether and under which conditions carrier multiplicaiton takes place in graphene. The many-particle-induced carrier generation can be quantified by a time-dependent carrier multiplication factor $\mathrm{CM(t)}$

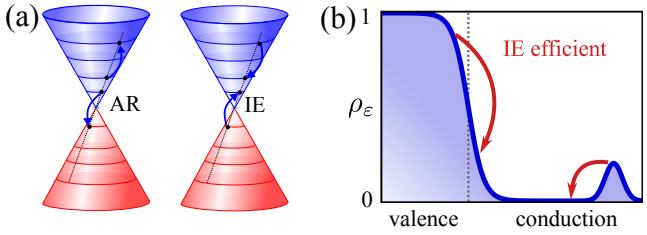

FIG. 1: Schematic illustration of Auger scattering processes including Auger recombination (AR) and the inverse process of impact excitation (IE). The latter can give rise to a carrier multiplication. Figure adapted from Ref.[2] and Ref.[4].

$$\mathrm{CM(t)} = \frac{\mathcal{N}(\mathrm{t})}{\mathcal{N}_{\mathrm{opt}}(\mathrm{t})}, \tag{1}$$

which is defined as the ratio of the generated carrier density $\mathcal{N}(t)$ and the purely optically excited density $\mathcal{N}_{opt}(t)$.

I. CARRIER MULTIPLICATION IN UNDOPED GRAPHENE

Here, we investigate the ultrafast carrier dynamics in undoped graphene. We find a significant increase of the carrier density $\mathcal{N}(t)$ after optical excitation, cf. Fig. 2. To understand the underlying microscopic mechanism, we subsequently switch on different scattering channels. Accounting only for carrier-light interaction, the applied ultrashort optical pulse lifts electrons from the valence into the conduction

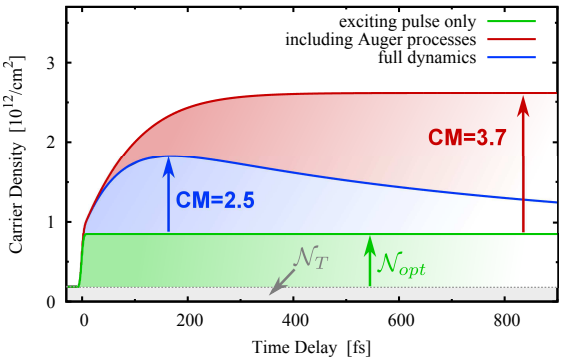

FIG. 2: Temporal evolution of the carrier density accounting for all relaxation channels (blue line), only carrier-light interaction (green line), and only Coulomb scattering (red). Auger scattering leads to a multiplication of the initially excited carrier density $\mathcal{N}_{\rm opt}$ by a factor of 3.7. Phonon-induced recombination counteracts the multiple charge carrier generation and reduces the CM factor to 2.5. Figure taken from Ref.[31]

band resulting in an optically induced carrier density $\mathcal{N}_{\rm opt}(t)$, which remains constant after the pulse is switched off (green line). Taking into account Coulomb-induced scattering channels including Auger processes, we find a further increase of the carrier density even after the pulse has been switched off (red line) - a carrier multiplication takes place. In the case of a purely Coulomb-driven dynamics, we obtain a multiplication factor of CM $= 3.7$. However, the dynamics is still uncomplete until we have included phonon-induced relaxation channels. These are important since they directly compete with Auger processes: an excited electron can scatter to an energetically lower state by emitting a phonon and thus reducing the efficiency of Auger scattering. Furthermore, phonon-induced interband processes can directly change the carrier density. Since non-radiative recombination involving the emission of phonons is efficient, it reduces the carrier density counteracting the effect of CM. In spite of these effects, taking the full dynamics into account we still observe a carrier multiplication with a maximum value of approximately CM $= 2.5$ that persists on a picosecond timescale, cf. the blue line in Fig. 2[3,4,32].

The theoretically predicted carrier multiplication in graphene could be recently also demonstrated in high-resolution multi-color pump-probe[17,19] and time-and angle-resolved photoemission (ARPES) measurements[24,25]. Direct experimental access to the temporal evolution of the carrier density in graphene is a challenging task. As absorption at optical frequencies is dominated by interband processes, pump-probe experiments can be used to directly monitor carrier occupation probabilities of the optically coupled states as well as the Coulomb- and phonon-induced carrier escape from these states. Ploetzing an co-workers[19] performed a series of pump-probe measurements applying different optical probe energies ranging from 0.73 to 1.6 eV, while the pump pulse was fixed at 1.6 eV. Assuming quasi-instantaneous thermalization of the excited carriers through ultrafast carrier-carrier scattering, the

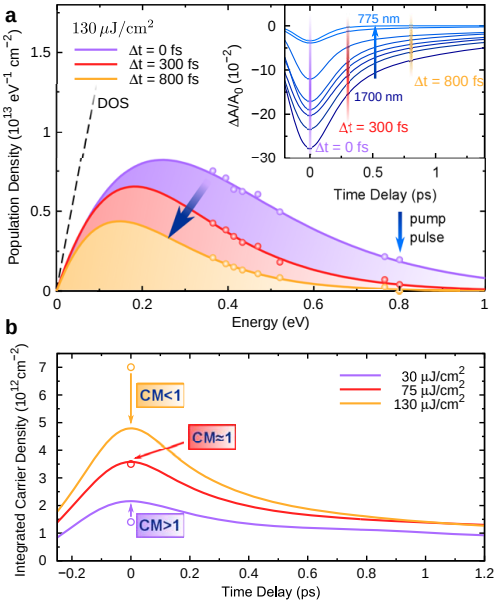

FIG. 3: (a) Thermalized carrier distributions at three different times, extracted from pump-probe measurements of the differential absorption $\Delta A/A_0$ (see inset) recorded at eight different probe wavelength for an excitation fluence of 130 μJ/cm^2. (b) Temporal evolution of the integrated carrier density after optical excitation at three different excitation fluences. The circles denote the estimated optically excited carrier density extracted from the applied pump fluence and the measured constant absorption of graphene on sapphire. Figure taken from Ref.[19].

measured occupation probabilities at different distinct energies could be exploited to reconstruct the time-dependent carrier distribution in the relevant range in the momentum space, cf. Fig. 3(a). To be able to draw qualitative conclusions on the appearing carrier multiplication, the optically excited carrier density $\mathcal{N}_{opt}$ is estimated based on the pump fluence and the dark absorption of graphene on sapphire. Depending on the pump fluence, $\mathcal{N}_{opt}$ lies below or above the intergrated carrier density $\mathcal{N}$, cf. Fig. 3(b). This is a clear experimental prove of the appearance of CM in graphene.

Figure 4 shows an excellent agreement between theory and experiment with respect to the appearance of the carrier multiplication, its quantitative values as well as its qualitative dependence on the pump fluence[19]. Since Auger processes are sensitive to the excited carrier density, the appearance of CM strongly varies in different excitation regimes. Depending on the pump fluence and the delay time after the optical pulse, we can clearly distinguish both in experiment and theory two distinct regions characterized by CM > 1 (purple) and CM < 1 (orange). We find the largest CM values at low pump fluences in the range of $0.1\,\mu$Jcm^{-2}. The CM appears on a timescale of several picoseconds. At intermediate pump fluences up to approximately $1\,\mu$Jcm^{-2}, we observe a smaller carrier multiplication on a much shorter timescale. Here, IE still prevails over AR, however the asymmetry between these two processes due to Pauli blocking is restricted to a shorter time range, since the number of scattering partners

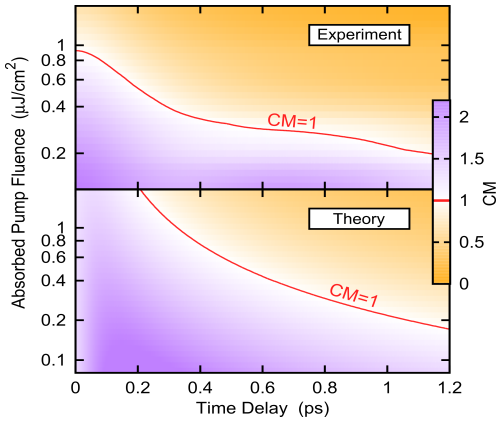

FIG. 4: Direct comparison of theoretically predicted and experimentally measured carrier multiplication. Purple colors mark the region characterized by a CM factor larger than 1, where the carrier density exceeds the density of optically injected carriers. Both in experiment and theory maximum carrier multiplication occurs at low fluences on a timescale of a few picoseconds. Figure taken from Ref.[19].

is increased accelerating the relaxation dynamics and leading to a faster equilibration between the IE and AR processes[4]. In the strong excitation regime with pump fluences larger than $1\,\mu\mathrm{Jcm}^{-2}$, the states are highly occupied and Pauli blocking preferes AR bringing carriers back to the valence band. As a result, the carrier density decreases and we find a *negative* carrier multiplication $\mathrm{CM} < 1$, cf. Fig. 4.

In addition to the multi-color pump-probe measurements, Gierz and co-workers[24] could demonstrate the presence of a strong impact excitation in a time-and angle-resolved photoemission spectroscopy study. Extreme-ultraviolet pulses were used to track the number of excited electrons and their kinetic energy. In a time window of approximately 25 fs after absorption of the pump pulse, a clear increase of carrier density and a simultaneous decrease of the average carrier kinetic energy was observed directly (cf. Fig. 5) revealing that relaxation is dominated by impact excitation.

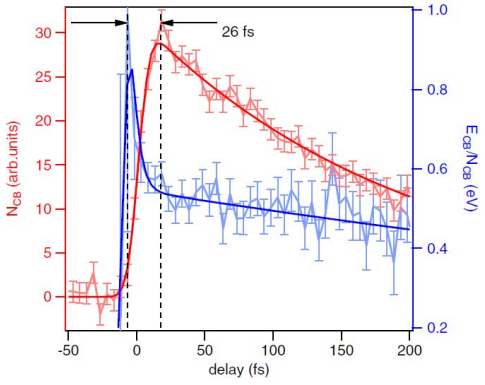

FIG. 5: Experimental prove for the predominant role of impact ionization in time-and angle-resolved photoemission (ARPES) measurements. Comparison between the temporal evolution of the total number of carriers inside the conduction band (light red) and the temporal evolution of their average kinetic energy (light blue). Around zero time delay, the energy already decreases while the number of carriers keeps revealing the importance of impact excitation. Figure taken from Ref.[24].

II. CARRIER MULTIPLICATION IN DOPED GRAPHENE

Most graphene samples are characterized by a non-zero doping, i.e. the Fermi energy lies above (n doping) or below the Dirac point (p doping). In this section, we investigate the influence of an extrinsic carrier density on the dynamics of optically excited carriers. Since doping breaks the symmetry between electrons and holes, we extend the graphene Bloch equations by deriving separate equations for the time evolution of electron occupations $\rho_{\mathbf{k}}^{e,c}$ in the conduction and and hole occupations $\rho_{\mathbf{k}}^{h,v}$ in the valence band. Furthermore, we include dynamic screening of the Coulomb potential accounting for the increased carrier density. Our calculations reveal that for n-doped (p-doped) graphene, electron (hole) relaxation is, as expected, faster resulting in a thermalized hot Fermi distribution already after 30 fs. This can be traced back to the increased number of scattering partners for electrons or holes depending on the type of doping[23].

In the presence of doping, we have to reconsider the definition of charge carriers. For n-doping, we can either count electrons above the Dirac point or above the Fermi level (for holes accordingly in p-doped samples). For optical measurements, probing vertical carrier transitions the Dirac point is the more appropriate reference. Then, the carrier density reads

$$\mathcal{N}_{\mathrm{CM}} = \frac{\sigma_s \sigma_v}{L^2} \sum_{\mathbf{k},\lambda=e,h} \rho_{\mathbf{k}}^{\lambda}, \tag{2}$$

where σ_s (σ_v) denotes the spin (valley) degeneracy and L^2 the graphene area. In contrast to optical measurements, for electric transport phenomena hot electrons around the Fermi level play the crucial role. Thus, charge carriers are defined with respect to the Fermi level, i.e. for n-doped graphene the upper Dirac cone is split into $\rho_{\mathbf{k}}^{h,c} = 1 - \rho_{\mathbf{k}}^{c}$ for $k < k_F$ and $\rho_{\mathbf{k}}^{e,c} = \rho_{\mathbf{k}}^{c}$ for $k > k_F$ with the Fermi momentum k_F. The bottom cone remains unaffected with $\rho_{\mathbf{k}}^{h,v} \equiv \rho_{\mathbf{k}}^{h} = 1 - \rho_{\mathbf{k}}^{v}$. The according *hot* carrier density $\mathcal{N}_{\mathrm{hCM}}$ is given by

$$\mathcal{N}_{\mathrm{hCM}} = \frac{\sigma_s \sigma_v}{L^2} \Big(\sum_{\mathbf{k}} \rho_{\mathbf{k}}^{h} + \sum_{\mathbf{k}}^{k<k_F} \rho_{\mathbf{k}}^{h,c} + \sum_{\mathbf{k}}^{k>k_F} \rho_{\mathbf{k}}^{e,c} \Big). \tag{3}$$

Note that symmetric results are obtained for n- and p-doped graphene. For undoped graphene, both definitions of carrier density and carrier multiplication are equivalent for symmetry reasons.

The definition of the charge carrier density has a direct impact on the appearance of carrier multiplication. Having the Dirac point as the reference, carrier multiplication occurs due to Auger scattering bridging the valence and the conduction band. In the following, we label this process as carrier multiplication (CM). Having the Fermi level as the reference, carrier multiplication occurs via Coulomb-induced intraband

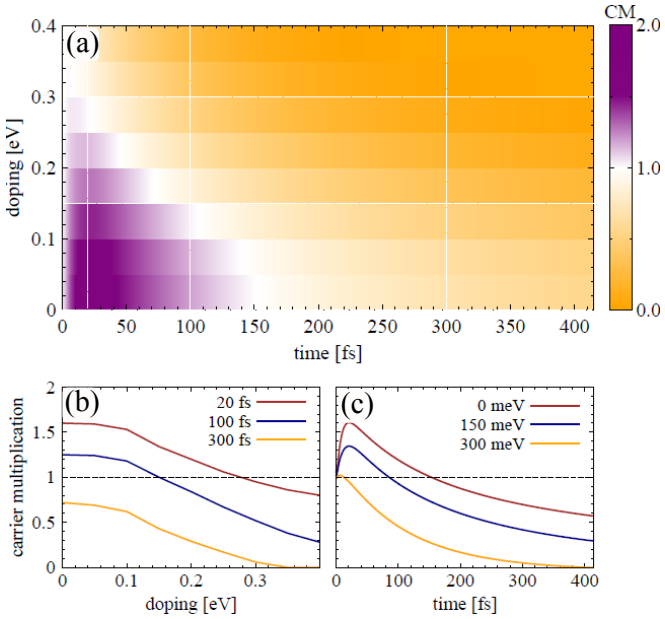

FIG. 6: Temporal evolution of the doping-dependent CM for a fixed absorbed pump fluence $\varepsilon_{\text{abs}} = 0.3\,\mu\text{Jcm}^{-2}$. (b) Doping-dependent CM for three fixed time delays and (c) the temporal evolution of CM for different doping levels. Figure taken from Ref.[23].

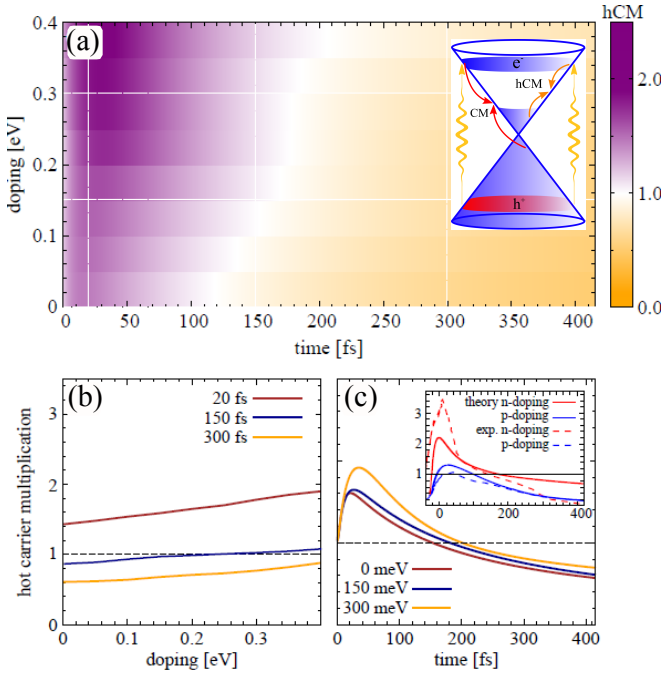

FIG. 7: The same investigation as in Fig. 6 for the case of hot carrier multiplication. The inset in (a) illustrates the processes responsible for CM and hCM in n-doped graphene. The inset in (f) shows a direct comparison between theoretically predicted (solid lines) and experimentally measured (dashed lines) data[25] for: (i) n-doped graphene ($E_F = 380\,\text{meV}$) with an absorbed pump fluence of $\varepsilon_{\text{abs}} = 0.5\,\mu\text{Jcm}^{-2}$ and (ii) p-doped graphene ($E_F = 240\,\text{meV}$) with a fluence of $\varepsilon_{\text{abs}} = 1.5\,\mu\text{Jcm}^{-2}$. Figure adapted from Ref.[23].

scattering bridging the states below and above the Fermi level, cf. the inset in Fig. 7(a). According to literature[33], we label this process as hot carrier multiplication (hCM).

We find that doping reduces the efficiency of CM, cf. Fig. 6(a). Considering an absorbed pump fluence of $\varepsilon_{\text{abs}} = 0.3\mu J$ cm^{-2}, the highest CM factor of 1.7 is obtained in the limiting case of undoped graphene, cf. Fig. 6(b). It appears on a timescale of up to 150 fs for undoped graphene and becomes significantly shorter with increasing doping, cf. Fig. 6(c). For doping values higher than 300 meV, CM completely vanishes. This behavior can be traced back to the strongly efficient impact excitation at low doping, which is a result of the large gradient in carrier occupation around the Dirac point. This changes for highly doped graphene presenting optimal conditions for the inverse process of Auger recombination.

In contrast, we predict a clear increase of the hCM with doping, cf. Fig. 7(a). We obtain hCM factors of up to approximately 2 occurring on a timescale of 200 fs for highly doped graphene with $E_F = 300\,\text{meV}$. There is nearly a linear dependence between hCM and doping, cf. Fig. 7(b). The intraband Coulomb scattering around the Fermi energy is responsible for the appearance of hCM. With increasing doping, the spectral region for these *intraband Auger processes* shifts to higher density of states. As a result, they become generally more efficient. The probability for *intraband IE processes* (inset in Fig. 7(a)) is given by $\rho^{h,c}(1-\rho^{e,c})$, which is initially large compared to the probability for *intraband AR processes* scaling with $\rho^{e,c}(1-\rho^{h,c})$. The initial strong imbalance between IE and AR gives rise to the observed pronounced hCM.

Applying our microscopic approach, we can explain the recently performed time-resolved ARPES measurements on n- and p-doped graphene[25]. A direct comparison of theoretically predicted and experimentally obtained values for hot carrier multiplication is shown in the inset of Fig. 7(c). The theory captures well all features observed in the experiment, such as the clearly higher hCM for n-doped graphene. This difference is not due to the type of doping, but can rather be explained by the differences in the applied pump fluence and the doping value of the investigated graphene samples. Hot carrier multiplication increases almost linearly with doping (cf. Fig. 7(b)) and becomes less efficient at high pump fluences (similarly to the case of CM, cf. Fig. 4). As a result, the n-doped graphene sample shows a much more pronounced hCM, since its Fermi level is significantly higher and since the experiment has been performed at a clearly smaller pump fluence compared to the p-doped graphene sample.

III. CARRIER MULTIPLICATION IN LANDAU-QUANTIZED GRAPHENE

Carrier multiplication holds the potential to increase the power conversion efficiency of photovoltaic devices. However, due to the absence of a bandgap and competing phonon-induced recombination, the extraction of charge carriers remains a substantial challenge. A strategy has been recently suggested to circumvent this drawback and to benefit from the gained charge carriers by introducing a Landau quantiza-

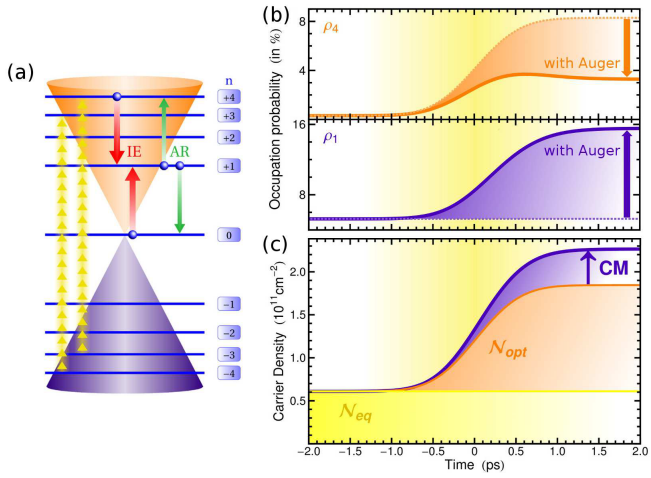

FIG. 8: (a) Illustration of the low-energetic Landau levels in graphene with the Dirac cone in the background, where the yellow arrows indicate the optical excitation. Carriers excited to LL +4 can participate in impact excitation (IE), which dominates over the inverse process of Auger recombination (AR). (b) Temporal evolution of the occupations ρ_{+4} and ρ_{+1} during an optical excitation. The dashed lines represent the dynamics in the absence of Auger scattering. The yellow region illustrates the width of the pump pulse. (c) Temporal evolution of the total carrier density $\mathcal{N}$ (purple line), the optically induced carrier density $\mathcal{N}_{opt}$ (orange line), and the constant equilibrium carrier density $\mathcal{N}_{\rm eq}$ (yellow line). Efficient impact excitation leads to a carrier multiplication of approximately 1.3. Figure taken from Ref.[18].

tion offering a tunable bandgap[18]. In the presence of magnetic fields the electronic bandstructure of graphene drastically changes. The Dirac cone collapses into discrete non-equidistant Landau levels, which can be externally tuned by changing the magnetic field[34–38]. In contrast to conventional materials, specific Landau levels are selectively addressable using circularly polarized light.

The first experiment measuring the carrier dynamics in Landau-quantized graphene was performed by Plochocka et al. in 2009[39]. Investigating rather high-energetic Landau levels ($n \sim 100$), they found a suppression of Auger processes as a consequence of the non-equidistant level spacings suggesting an overall suppression of Auger processes in Landau-quantized graphene[39]. However, due to the $E \propto \sqrt{n}$ dependence, we can always find Landau levels n that are actually equidistant suggesting that Auger scattering might be important in certain situation. This has been confirmed in a recent polarization-resolved pump-probe experiment addressing the crucial impact of Auger scattering to the low-energetic Landau levels[26].

Recently, we have suggested a pumping scheme to open up Auger scattering channels and to achieve a carrier multiplication in Landau-quantizede graphene, cf. Fig. 8(a). The strategy is to excite charge carriers to LL +4, which induces an energy conserving scattering process including the transitions LL +4 $\rightarrow$ LL +1 and LL 0 $\rightarrow$ LL +1. This process is denoted as impact excitation (IE), since it effects the excitation of an additional charge carrier. Due to Pauli blocking, we expect the inverse process of Auger recombination (AR) to be suppressed.

To investigate the impact of Auger scattering and to prove whether CM appears, we calculate the temporal evolution of the carrier occupation of the involved Landau levels LL +4 and LL +1, cf. Fig. 8(b). The applied optical pulse is characterized by a width $\sigma^{\rm exp}_{\rm FWHM} = 1\,$ps (yellow shaded region), pump fluence $\varepsilon_{\rm pf} = 10^{-2}\,\mu$Jcm^{-2}, and an energy 280 meV matching the transitions LL $\mp$ 4 $\rightleftarrows$ LL $\pm$ 3 at a magnetic field of $B = 4\,$T. The system is considered to be at room temperature and an impurity-induced Landau level broadening of $\Gamma^{\rm imp} = 7\,$meV is assumed. The dashed lines in Fig. 8(b) represent the dynamics without Auger scattering. In this case, the occupation ρ_{+4} simply increases during the optical excitation, while ρ_{+1} stays constant, since it is not optically excited. Switching on Auger processes (solid lines) results in a considerable transfer of occupation from LL +4 to LL +1. The total increase of ρ_{+1} (about 10%) exceeds the decrease of ρ_{+4} (about 5%) by a factor of 2. This reflects the predominant process of impact excitation inducing the transitions LL +4 $\rightarrow$ LL +1 and LL 0 $\rightarrow$ LL +1, cf. the red arrows in Fig. 8(a).

Figure 8(c) shows the temporal evolution of the carrier density revealing a clear increase due to the efficient impact excitation. As a result, a carrier multiplication of 1.3 appears in Landau-quantized graphene. Note that the maximal CM that can be achieved within the proposed pumping scheme is 1.5. However, an optical excitation into a higher energetic Landau level is conceivable and is expected to induce higher values of the CM. In general, a low pump fluence is advantageous for CM, since a stronger optical excitation results in an increased asymmetry between the competing IE and AR scattering channels, leading to a faster equilibration of the corresponding scattering rates and reducing the time frame in which IE generates additional charge carriers. Moreover, changes of the initial occupations result in an increasing CM with lower temperatures and higher magnetic fields. Additionally, the CM increases with the magnetic field, as the effective pumping strength is reduced. Finally, a higher value of the CM is obtained for larger Landau level broadenings.

The theoretically predicted importance of Auger scattering in Landau-quantized graphene is remarkable due to the non-equidistant level separation. Luckily, the carrier occupation of single LLs can be directly addressed via polarization-dependent pump-probe experiments allowing an experimental investigation of the importance of Auger channels. Using circularly polarized light of a specific energy, we can selectively pump and probe transitions between the energetically lowest Landau levels LL -1, LL 0 and LL +1. This results in four possibilities to combine pump and probe pulse polarization, cf. Fig. 9. Considering only the optical excitation, we expect a positive differential transmission signal (DTS), if the pump σ_P and the probe (test) pulse σ_T have the same polarization. Here, the excitation of charge carriers due to the pump pulse should lead to an absorption bleaching of the probe pulse due to the increased Pauli blocking. In contrast, using an opposite polarization for the pump and the probe pulse, Pauli blocking

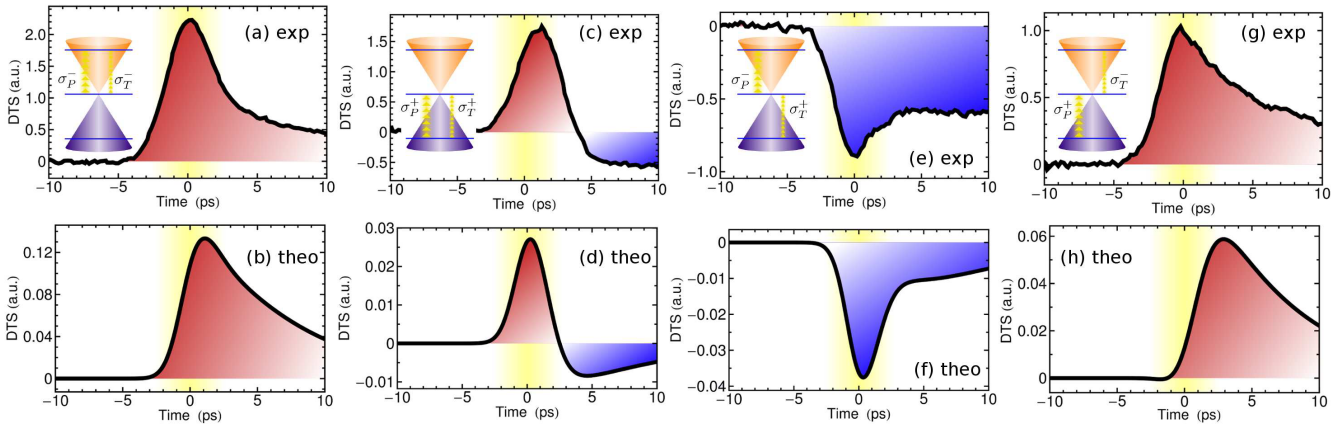

FIG. 9: Direct comparison of experimentally measured (upper panel) and theoretically predicted (lower panel) polarization-resolved differential transmission for pumping and probing the same transition [(a)-(d)] and different transitions [(e)-(h)]. The corresponding pump (σ_{P}) and probe (or test σ_{T}) pulses are sketched in the insets. The yellow shaded areas in the background illustrate the width of the pump pulse. Figure adapted from Ref.[30].

is expected to be reduced giving rise to an absorption enhancement and a negative DTS.

The upper and lower panel of Fig. 9 illustrate the experimental and theoretical results, respectively, for the four configurations of pump and probe pulse polarization applying a pulse with a width of $\sigma_{\mathrm{FWHM}}^{\mathrm{exp}} = 2.7\,\mathrm{ps}$ and an energy of $75\,\mathrm{meV}$. Comparing the data with the expectation based on the occupation change induced by the optical excitation, a qualitative difference is observed both in experiment and theory in the case of pumping with σ^--polarized radiation (Figs. 9(e)-(h)): While the configuration σ_{P}^-, σ_{T}^- shows an initial increase (as expected) which is followed by an unexpected sign change to the negative region, the measured behavior in the configuration σ_{P}^-, σ_{T}^+ is completely contrary to what we would expect.

To explain these surprising results, we need to take into account Auger scattering. Moreover, to achieve an agreement between experiment and theory, a finite doping needs to be introduced to break the electron-hole symmetry. In an undoped system, the two configurations σ_{P}^+, σ_{T}^+ and σ_{P}^-, σ_{T}^- (and likewise σ_{P}^+, σ_{T}^- and σ_{P}^-, σ_{T}^+) would yield the same result. The assumption of a finite doping is further supported by experimental studies showing that multilayer epitaxial graphene samples grown on the C-terminated face of SiC (such a sample is used in the experiment) have a finite n-doping due to a charge transfer from the SiC substrate[40,41]. Therefore, for the theoretical calculations a Fermi energy of $\varepsilon_{\mathrm{F}} = 28\,\mathrm{meV}$ has been assumed.

To understand the unexpected DTS sign in Fig. 9(g), we investigate the temporal evolutions of the involved Landau level occupations ρ_{+1}, ρ_0 and ρ_{-1} after the application of a σ^--polarized pump pulse, cf. Fig. 10(a). To identify the role of Auger scattering, we compare the full dynamics with the calculation without Auger processes, cf. the dashed gray line. Note that carrier-phonon scattering has been phenomenologically included to match the experimentally observed fast decay rates at long times. Although the transition LL -1 $\rightarrow$ LL 0 is optically induced, the occupation ρ_0 shows only a minor increase in the beginning, then it starts even to decrease already before the center of the pulse is reached. This means that although we optically pump carriers into the zeroth Landau level, its population decreases. This surprising result can be explained by extremely efficient Auger scattering, which induces the transitions LL 0 $\rightarrow$ LL -1 and LL 0 $\rightarrow$ LL +1, thereby resulting in a quick depopulation of ρ_0, cf. Fig. 10(b). The crucial role of the Auger scattering becomes apparent by comparing the temporal evolution of ρ_0 to the case without Coulomb scattering (cf. dashed gray lines in Fig. 10(a). Here, as expected, the population of the zeroth Landau level increases during the entire time of the optical excitation.

As a result, the polarization-dependent pump-probe experiments provide proof for efficient Auger scattering in Landau-quantized graphene. The unexpected DTS sign emerges since

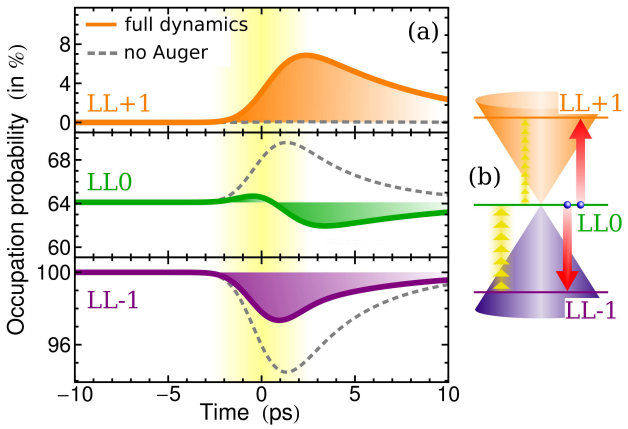

FIG. 10: (a) Temporal evolution of the three energetically lowest Landau involved in the Auger processes from Fig. 9 after a σ^--polarized excitation. (b) The sketch illustrates the interplay of Auger scattering and optical excitation explaining that Auger scattering can even lead to a depopulation of the zeroth Landau level even though carriers are pumped into this level. Figure adapted from Ref.[26].

Auger scattering depopulates the zeroth Landau level faster than it is filled by optical excitation. This surprising effect appears, when the pumping efficiency is decreased due to an enhanced Pauli blocking as a result of a finite doping.

In summary, we have reviewed the current research on carrier multiplication in undoped, doped, and Landau-quantized graphene. We find that Auger scattering bridging the valence and the conduction band dominates the carrier dynamics in graphene. In particular, impact excitation is the predominant relaxation channel under certain conditions resulting in a significant carrier multiplication.

We thank our experimental collaborators, in particular Stephan Winnerl and Manfred Helm (Helmholtz-Zentrum Dresden-Rossendorf) as well Daniel Neumeier and Heinrich Kurz (AMO Aachen). Furthermore, we acknowledge financial support from the Deutsche Forschungsgemeinschaft (DFG) through the priority programm 1458, the EU Graphene Flagship (contract no. CNECT-ICT-604391), and the Swedish Research Council (VR).

* ermin.malic@chalmers.se

[1] A.J Nozik. Quantum dot solar cells. *Physica E*, 14:115 – 120, 2002.

[2] Ermin Malic, Stephan Winnerl, and Andreas Knorr. *Graphene and Carbon Nanotubes: Ultrafast Optics and Relaxation Dynamics*. Wiley-VCH, 1 edition, May 2013.

[3] Torben Winzer, Andreas Knorr, and Ermin Malic. Carrier multiplication in graphene. *Nano Letters*, 10(12):4839–4843, December 2010.

[4] Torben Winzer and Ermin Malić. Impact of auger processes on carrier dynamics in graphene. *Physical Review B*, 85(24):241404, June 2012.

[5] R. D. Schaller and V. I. Klimov. High Efficiency Carrier Multiplication in PbSe Nanocrystals: Implications for Solar Energy Conversion. *Phys. Rev. Lett.*, 92:186601, 2004.

[6] R. D. Schaller, V. M. Agranovich, and V. I. Klimov. High-efficiency carrier multiplication through direct photogeneration of multi-excitons via virtual single-exciton states. *Nature Phys.*, 1:189–194, 2005.

[7] Randy J. Ellingson, Matthew C. Beard, Justin C. Johnson, Pingrong Yu, Olga I. Micic, Arthur J. Nozik, Andrew Shabaev, and Alexander L. Efros. Highly Efficient Multiple Exciton Generation in Colloidal PbSe and PbS Quantum Dots. *Nano Lett.*, 5:865–871, 2005.

[8] Ilan Gur, Neil A. Fromer, Michael L. Geier, and A. Paul Alivisatos. Air-Stable All-Inorganic Nanocrystal Solar Cells Processed from Solution. *Science*, 310(5747):462–465, 2005.

[9] Gregory D. Scholes and Garry Rumbles. Excitons in nanoscale systems. *Nat. Mater.*, 5(9):683–696, September 2006.

[10] R. D. Schaller, M. Sykora, J. M. Pietryga, and V. I. Klimov. Seven Excitons at a Cost of One: Redefining the Limits for Conversion Efficiency of Photons into Charge Carriers. *Nano Lett.*, 6:424–429, 2006.

[11] G. Nair, L.-Y. Chang, S. M. Geyer, and M. G. Bawendi. Perspective on the Prospects of a Carrier Multiplication Nanocrystal Solar Cell. *Nano Lett.*, 11:2145–2151, 2011.

[12] Nathaniel M. Gabor, Zhaohui Zhong, Ken Bosnick, Jiwoong Park, and Paul L. McEuen. Extremely efficient multiple electron-hole pair generation in carbon nanotube photodiodes. *Science*, 325(5946):1367–1371, September 2009.

[13] Roi Baer and Eran Rabani. Can impact excitation explain efficient carrier multiplication in carbon nanotube photodiodes? *Nano Letters*, 10(9):3277–3282, September 2010.

[14] Haining Wang, Jared H. Strait, Paul A. George, Shriram Shivaraman, Virgil B. Shields, Mvs Chandrashekhar, Jeonghyun Hwang, Farhan Rana, Michael G. Spencer, Carlos S. Ruiz-Vargas, and Jiwoong Park. Ultrafast relaxation dynamics of hot optical phonons in graphene. *Applied Physics Letters*, 96(8):081917–081917–3, February 2010.

[15] N. M. Gabor. Impact excitation and electron-hole multiplication in graphene and carbon nanotubes. *Acc. Chem. Res.*, 46:1348, 2013.

[16] Y. Kanemitsu. Multiple Exciton Generation and Recombination in Carbon Nanotubes and Nanocrystals. *Acc. Chem. Res.*, 46:1358–1366, 2013.

[17] D. Brida, A. Tomadin, C. Manzoni, Y. J. Kim, A. Lombardo, S. Milana, R. R. Nair, K. S. Novoselov, A. C. Ferrari, G. Cerullo, and M. Polini. Ultrafast collinear scattering and carrier multiplication in graphene. *Nature Commun.*, 4:1987, 2013.

[18] Florian Wendler, Andreas Knorr, and Ermin Malic. Carrier multiplication in graphene under Landau quantization. *Nature Commun.*, 5:3703, 2014.

[19] T. Plötzing, T. Winzer, E. Malic, D. Neumaier, A. Knorr, and H. Kurz. Experimental Verification of Carrier Multiplication in Graphene. *Nano Lett.*, 14(9):5371–5375, 2014. PMID: 25144320.

[20] P. T. Landsberg, H. Nussbaumer, and G. Willeke. Band-band impact ionization and solar cell efficiency. *J. Appl. Phys.*, 74:1451–1452, 1993.

[21] William Shockley and Hans J. Queisser. Detailed balance limit of efficiency of p-n junction solar cells. *Journal of Applied Physics*, 32(3):510–519, March 1961.

[22] D. M. Basko. Effect of anisotropic band curvature on carrier multiplication in graphene. *Phys. Rev. B*, 87:165437, 2013.

[23] F. Kadi, T. Winzer, A. Knorr, and E. Malic. Impact of doping on the carrier dynamics in graphene. *Sci. Rep.*, 5:16841, 2015.

[24] I. Gierz, F. Calegari, S. Aeschlimann, M. Chavez Cervantes, C. Cacho, R. T. Chapman, E. Springate, S. Link, U. Starke, C. R. Ast, and A. Cavalleri. Tracking primary thermalization events in graphene with photoemission at extreme timescales. *Phys. Rev. Lett.*, 115:086803, 2015.

[25] Jens Christian Johannsen, Søren Ulstrup, Alberto Crepaldi, Federico Cilento, Michele Zacchigna, Jill A. Miwa, Cephise Cacho, Richard T. Chapman, Emma Springate, Felix Fromm, Christian Raidel, Thomas Seyller, Phil D. C. King, Fulvio Parmigiani, Marco Grioni, and Philip Hofmann. Tunable carrier multiplication and cooling in graphene. *Nano Letters*, 15(1):326–331, 2015. PMID: 25458168.

[26] M. Mittendorff, F. Wendler, E. Malic, A. Knorr, M. Orlita, M. Potemski, C. Berger, W. A. de Heer, H. Schneider, M. Helm, and S. Winnerl. Carrier dynamics in Landau-quantized graphene featuring strong Auger scattering. *Nature Phys.*, 11:75–81, 2015.

[27] A. Knorr, S. Hughes, T. Stroucken, and S. W. Koch. Theory of ultrafast spatio-temporal dynamics in semiconductor heterostructures. *Chemical Physics*, 210:27 – 47, 1996.

[28] Ermin Malic, Torben Winzer, Evgeny Bobkin, and Andreas Knorr. Microscopic theory of absorption and ultrafast many-particle kinetics in graphene. *Physical Review B*, 84(20):205406, November 2011.

[29] Ermin Malic, Torben Winzer, Florian Wendler, and Andreas

Knorr. *Microscopic view on ultrafast carrier dynamics in graphene, in Optical Properties of Graphene, ed. by R. Binder*. World Scientific, 2016.

[30] Florian Wendler, Andreas Knorr, and Ermin Malic. Ultrafast carrier dynamics in landau-quantized graphene. *Nanophotonics*, 4(1):224–249, 2015.

[31] T. Winzer. *Ultrafast Carrier Relaxation Dynamics in Graphene*. PhD thesis, Technische Universität Berlin, July 2013.

[32] Torben Winzer and Ermin Malic. Carrier multiplication and optical gain in graphene. Proc. SPIE, page 8984, 2014.

[33] K. J. Tielrooij, J. C. W. Song, S. A. Jensen, A. Centeno, A. Pesquera, A. Zurutuza Elorza, M. Bonn, L. S. Levitov, and F. H. L. Koppens. Photoexcitation cascade and multiple hot-carrier generation in graphene. *Nature Physics*, 9:248, February 2013.

[34] F. D. M. Haldane. Model for a Quantum Hall Effect without Landau Levels: Condensed-Matter Realization of the "Parity Anomaly". *Phys. Rev. Lett.*, 61:2015–2018, 1988.

[35] M. L. Sadowski, G. Martinez, M. Potemski, C. Berger, and W. A. de Heer. Landau Level Spectroscopy of Ultrathin Graphite Layers. *Phys. Rev. Lett.*, 97:266405, 2006.

[36] P. Plochocka, C. Faugeras, M. Orlita, M. L. Sadowski, G. Martinez, M. Potemski, M. O. Goerbig, J.-N. Fuchs, C. Berger, and W. A. de Heer. High-Energy Limit of Massless Dirac Fermions in Multilayer Graphene using Magneto-Optical Transmission Spectroscopy. *Phys. Rev. Lett.*, 100:087401, 2008.

[37] M. Orlita, C. Faugeras, P. Plochocka, P. Neugebauer, G. Martinez, D. K. Maude, A.-L. Barra, M. Sprinkle, C. Berger, W. A. de Heer, and M. Potemski. Approaching the Dirac Point in High-Mobility Multilayer Epitaxial Graphene. *Phys. Rev. Lett.*, 101:267601, 2008.

[38] David L. Miller, Kevin D. Kubista, Gregory M. Rutter, Ming Ruan, Walt A. de Heer, Phillip N. First, and Joseph A. Stroscio. Observing the Quantization of Zero Mass Carriers in Graphene. *Science*, 324:924–927, 2009.

[39] P. Plochocka, P. Kossacki, A. Golnik, T. Kazimierczuk, C. Berger, W. A. de Heer, and M. Potemski. Slowing hot-carrier relaxation in graphene using a magnetic field. *Phys. Rev. B*, 80:245415, 2009.

[40] M. Sprinkle, D. Siegel, Y. Hu, J. Hicks, A. Tejeda, A. Taleb-Ibrahimi, P. Le Fèvre, F. Bertran, S. Vizzini, H. Enriquez, S. Chiang, P. Soukiassian, C. Berger, W. A. de Heer, A. Lanzara, and E. H. Conrad. First Direct Observation of a Nearly Ideal Graphene Band Structure. *Phys. Rev. Lett.*, 103:226803, 2009.

[41] Dong Sun, Charles Divin, Julien Rioux, John E. Sipe, Claire Berger, Walt A. de Heer, Phillip N. First, and Theodore B. Norris. Coherent control of ballistic photocurrents in multilayer epitaxial graphene using quantum interference. *Nano Letters*, 10(4):1293–1296, April 2010.